Incision of submarine channels over pockmark trains in the South China Sea

Kaiqi Yu [1, 2, 3], Elda Miramontes [4, 5], Tiago M. Alves [6], Wei Li [1, 2, 3] *, Linlin Liang [3, 7], Shuang Li [1, 2, 3], Wenhuan Zhan[1, 2, 3], Shiguo Wu [3, 8]

[1]Key Laboratory of Ocean and Marginal Sea Geology, South China Sea Institute of Oceanology, Innovation Academy of South China Sea Ecology and Environmental Engineering, Chinese Academy of Sciences, Guangzhou 510301, China.

[2]Southern Marine Science and Engineering Guangdong Laboratory (Guangzhou), Guangzhou 511458, China.

[3]University of Chinese Academy of Sciences, Beijing 100049, China.

[4]Faculty of Geosciences, University of Bremen, Bremen 28359, Germany.

[5]MARUM-Center for Marine Environmental Sciences, University of Bremen, Bremen, 28359, Germany.

[6]3D Seismic Laboratory, School of Earth and Environmental Sciences, Cardiff University, Main Building, Park Place, Cardiff, CF10 3AT, United Kingdom.

[7]State Key Laboratory of Tropical Oceanography, South China Sea Institute of Oceanology, Chinese Academy of Sciences, Guangzhou, China.

[8]Institute of Deep-sea Science and Engineering, Chinese Academy of Sciences, Sanya, 572000, China

*Corresponding authors: Dr. Wei Li (wli@scsio.ac.cn)

Key Points:

- A complex system of channels in the western South China Sea was formed by the erosion of seafloor pockmarks.
- The evolution from pockmark to submarine channel comprises three stages: pockmark train, immature, and mature channel.
- This on-going system of channels was initiated in the Late Miocene and was significantly influenced by seafloor topography.

Abstract

The genesis of submarine channels is often controlled by gravity flows, but they can also be formed by oceanographic processes. Using multibeam bathymetric and two-dimensional seismic data from the western South China Sea, this work reveals how pockmarks ultimately form channels under the effect of bottom currents and gravity processes. We demonstrate that alongslope and across-slope channels were initiated by pockmark trains on the seafloor. Discrete pockmarks were elongated due to the erosion of gravity processes and bottom currents, and later coalesced to form immature channels with irregular thalwegs. These gradually evolved into mature channels with continuous overbanks and smooth thalwegs. Submarine channel evolution was significantly influenced by seafloor topography since the Late Miocene. The evolutionary model documented here is key to understanding how channels are formed in deep-water environments.

Plain Language Summary

Submarine channels are prominent erosional features on continental slopes and basin floors. They are usually formed by submarine sea currents and sediment avalanches flowing downslope. Here, we investigate a system of channels on the western South China Sea using geophysical methods. The channels are formed in a region with widespread seafloor depressions (pockmarks) reflecting the seepage of fluid into the water column. Gravity-driven sedimentary processes and ocean currents reshaped these pockmarks, which were ultimately merged together to form immature and irregular channels. Under continued erosion, the immature channels eventually developed mature channels with continuous overbanks and smooth channel floors. This study reveals that ocean currents and gravity processes can form channels with different orientations by eroding pre-existing pockmarks.

1. Introduction

Submarine channels are erosional features that can be several km-wide and 10s to 100s km-long and are commonly found on continental margins and abyssal plains (Fildani et al., 2013; Hansen et al., 2017; Lemay et al., 2020). They are important elements of source-to-sink depositional systems, and can gather abundant paleoceanographic and paleoclimatic information in their constituent channel-fill deposits (Hernández-Molina et al., 2003; Zhu et al., 2010; Allen, 2017). The generation of channels transverse to continental slopes is mainly controlled by gravitational processes (Fildani et al., 2013; Li et al., 2015; de Leeuw et al., 2016), but can also be influenced by oceanographic processes such as dense shelf-water cascading and internal waves (Puig et al., 2014). In contrast, contour currents are the primary control on the evolution of submarine channels parallel to the slope bathymetry (Rebesco et al., 2014; García et al., 2009; Stow et al., 2013; Miramontes et al., 2020; 2021).

Large numbers of crater-like depressions co-exist with channels in regions such as the Gulf of Cadiz (León et al., 2010), West Africa (Pilcher and Argent, 2007), Mediterranean Sea (Miramontes et al., 2019), and New Zealand (Hillman et al., 2018).

These crater-like depressions comprise seafloor pockmarks generated by the erosional power of focused fluid vents on soft sediment (Hovland et al., 2002; Dandapath et al., 2010). Their size and shape depend on the activity of the fluid seeping through them, the grain size of near-seafloor sediment, and the erosional power of currents (Gay et al., 2007). Importantly, seafloor pockmarks can also be reshaped by downslope and alongslope processes to form pockmark-related morphologies such as gullies, furrows and comet structures (León et al., 2010; Kilhams et al., 2011).

Despite the above, it is still unclear whether pockmarks can evolve into channels, and which processes control their morphology. In order to decipher the latter processes, this study aims to: (1) characterize the morphology and internal architecture of channels in a poorly studied part of the South China Sea; (2) reconstruct the initiation and interpret the processes controlling the development of the investigated channels; and (3) reveal the role of pockmarks in submarine channel incision. The Western South China Sea is an ideal region to study the evolution of pockmarks because their origin is well known (Lu et al., 2017), and submarine channels with different orientations and sizes are abundant (Figure 1).

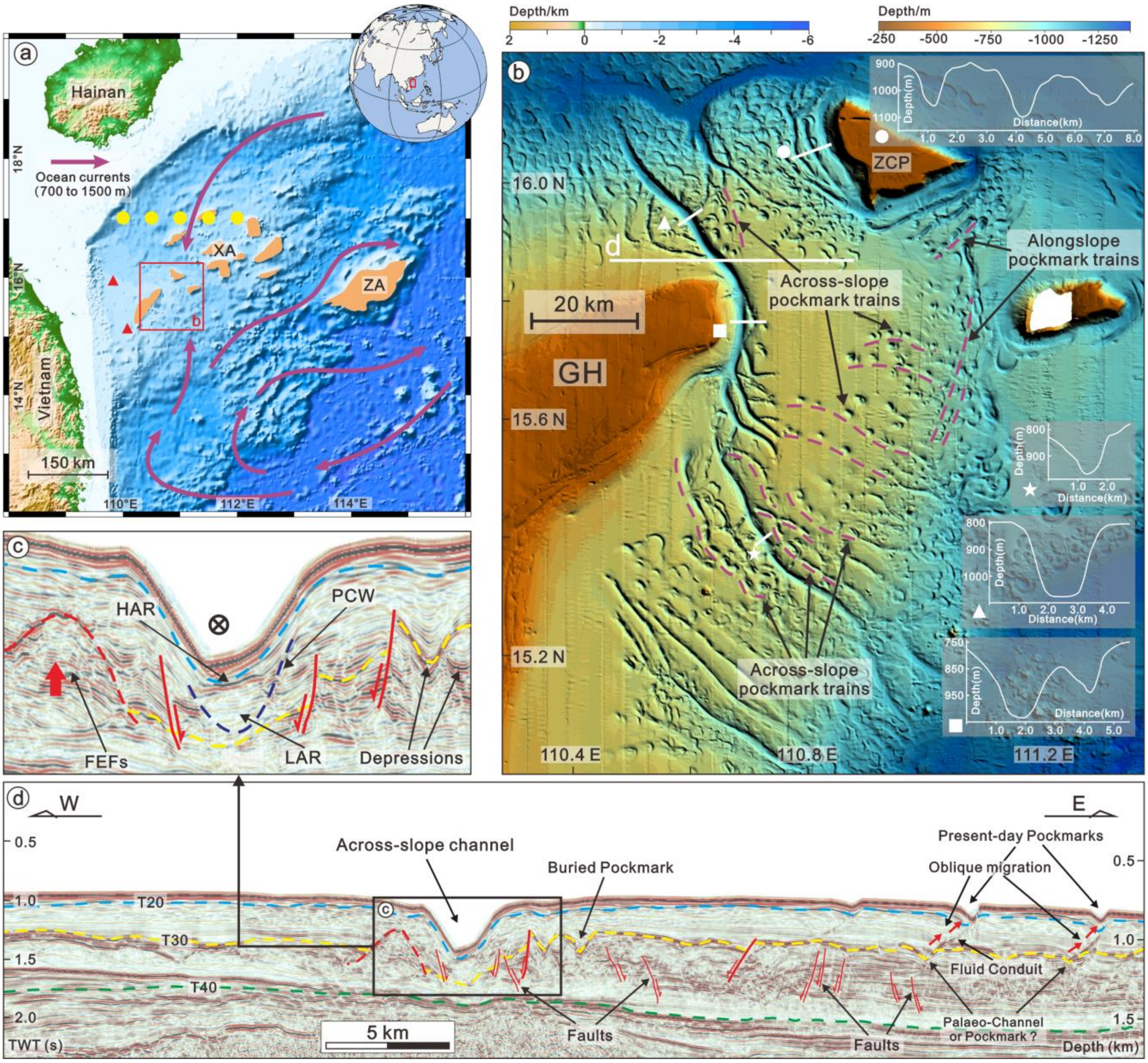

Figure 1. Location, oceanography and seismic-stratigraphic markers of the study area. a) Bathymetric map of the western South China Sea revealing the location of the study area. The purple arrows indicate the circulation direction at a water depth of 700-1500 m based on Quan et al. (2018). The yellow dots indicate the location of the speed profiles for the ocean currents shown in Figure S9 of the supporting information that were acquired with a vessel-mounted ADCP (2009-2012) and published by Yang et al. (2019). The red triangles show the location of sediment cores collected for grain size analysis of sea-bottom sediments (Astakhov, 2004a; b). XA and ZA indicate the location of the Xisha and Zhongsha Archipelagos, respectively. b) Multibeam bathymetric map showing the submarine channels and pockmarks studied in this work. Bathymetric profiles show the geometry of channel cross-sections. The purple dashed lines indicate the tracks of across-slope and alongslope pockmark trains. GH: Guangle High; ZCP: Zhongjianbei Carbonate Platform. c) A zoomed-in inset of seismic profile shows the internal architecture of an across-slope channel. d) Two-dimensional seismic

profile showing regional stratigraphic units (based on Lu et al., 2017), and main structures around the studied channel system. The dashed dark-blue line reveals the base and wall of the oldest paleo-channel observed under a modern submarine channel. Seismic horizons T20, T30 and T40 correlate with the bases of Quaternary, Pliocene and Late Miocene strata, respectively.

2. Materials and Methods

High-resolution multibeam bathymetric data and two-dimensional (2D) multi-channel seismic reflection profiles are used in this study. The multibeam bathymetric data were acquired in 2008 by the Guangzhou Marine Geological Survey (GMGS) using a SeaBeam 2112 system, which covered an area of ~10,000 km^2 at a water depth ranging from 300 m to 1300 m. These bathymetric data have a horizontal resolution of ~100 m (cell size) and a vertical resolution of ~3 m (3‰ of the water depth). The data were imported and analyzed in Global Mapper®.

Two-dimensional (2D) seismic reflection data were acquired by the China National Petroleum Company (CNPC) in 2005 and processed by the PetroChina Hangzhou Research Institute of Geology. The data were migrated with a common midpoint (CMP) spacing of 12.5 m and a main frequency bandwidth of 30 Hz to 45 Hz (main frequency: 35 Hz). The vertical resolution of the seismic data approaches 25 m. The 2D seismic data were interpreted on Landmark®. The ages of main seismic stratigraphic markers were based on Lu et al. (2017).

In order to provide a reference about the typical values of current velocity in the western South China Sea, we show in Figure S9 of the supporting information the average currents along a transect (see location in Fig. 1a) during four different years (2009, 2010, 2011 and 2012). Current measurements were acquired using a vessel-mounted ADCP Ocean Surveyor 38kHz (OS38) and were published by Yang et al. (2019).

3. Regional setting

3.1. Geological setting

The South China Sea was formed from Oligocene to the middle Miocene and is the largest (~3.5 ×10^6 km^2) and deepest (> 5000 m) marginal sea in the western Pacific Ocean (Zhou et al., 1995; Li et al., 2014). The study area lies southwest of the Xisha Archipelago on a topographic high identified between two drowned carbonate platforms, the Guangle High (GH) and the Zhongjianbei Carbonate Platform (ZCP) (Figure 1b). Pockmarks are abundant and relate to regional hydrothermal activity and gas seepage (Lu et al., 2017; Gao et al., 2019). Sediment cores collected to the west of the study area (Figure 1a) indicate that bottom sediment is composed of silt, with the particle diameter representing the 50% cumulative percentile value (D50) ranging between 5 and 50 μm (Astakhov, 2004a; b; Figure 1a).

This study focuses on the shallow strata of the western South China Sea, which can be subdivided into three seismic-stratigraphic units: Unit 1 (Quaternary); Unit 2

(Pliocene) and Unit 3 (Late Miocene). The bases of these units correlate with seismic horizons of T20, T30 and T40, respectively (Figures 1d and S1). The seismic-stratigraphy of the study area is interpreted based on regional correlations with adjacent regions (Lu et al., 2017).

3.2. Oceanographic setting

The South China Sea is a semi-enclosed marginal sea connected to the Pacific Ocean through the Luzon Strait (Liu et al., 2008). At present, the western South China Sea comprises four main water masses: surface water (at a water depth between 0 and 750 m), intermediate water (at water depths between 750 and 1500 m), deep and bottom waters deeper than 1500 m (Quan and Xue, 2018; Yin et al., 2021). Quan and Xue (2018) proposed a layered circulation model for the western South China Sea, in which current direction between 700 and 1500 m water depth is to the south in the northern part of the study area, but changing to a northward direction in the southern part (Figure 1a). According to the vessel-mounted ADCP data from Yang et al. (2019), ocean currents close to the study area show a variable behavior, with their average speed ranging from 10 to 20 cm/s. The measured maximum speed of ocean currents reaches 80 cm/s (Figures 1a and S9).

4. Giant pockmark field

A giant pockmark field covering an area of more than 9,000 km^2 is recognized on the multibeam bathymetric map in Figure 1b. Pockmarks are widespread and are generally arranged in continuous trains of pockmarks (Figures 1b and 2a). These pockmark trains are divided into two main categories: alongslope and across-slope. Pockmark trains that are parallel to the regional bathymetric contours, or located around bathymetric highs, are herein named “alongslope pockmark trains”. This category includes pockmarks formed around the ZCP and in the eastern part of study area (Figures 1b and 2b). The second category is named “across-slope pockmark trains” and comprises those aligned in a trend perpendicular to the bathymetric contours (Figure 1b). Across-slope pockmark trains are observed in the slopes south, east and north of the GH, at a water depth ranging from 750 to 900 m (Figures 1b and 2a).

Bathymetric data reveal that pockmarks are diverse in their geometry and dimensions (Figures 2 and S8). Pockmark depth oscillates between 50 and 180 m, with a maximum diameter from 1 to 3 km (Figure S8). Pockmarks are also variable in plan-view comprising elongated, comet-shaped, circular and crescent-shaped features (Figures 1b, 2b and 2c). Circular pockmarks are relatively small and often isolated when compared to the three other types, revealing pockmark width between 0.8 and 1.5 km (Figures 2c and S8). Crescent pockmarks are shaped as slender curves and distributed in groups; their concave side is aligned in the same direction (Figure 2b). Comet-shaped and elongated pockmarks are 1-3 km wide and 80-170 m deep, values that are similar to the bankfull width and height of adjacent submarine channels. They are usually aligned and show a consistent orientation (Figures 2b and 2c).

Seismic profiles reveal that most pockmarks are formed during or after the Pliocene, as they occur above or truncate horizon T30 (Figures 1d and 3), with only a few forming before the Pliocene (Figure S6). This is a character further discussed in Section 6 of this paper.

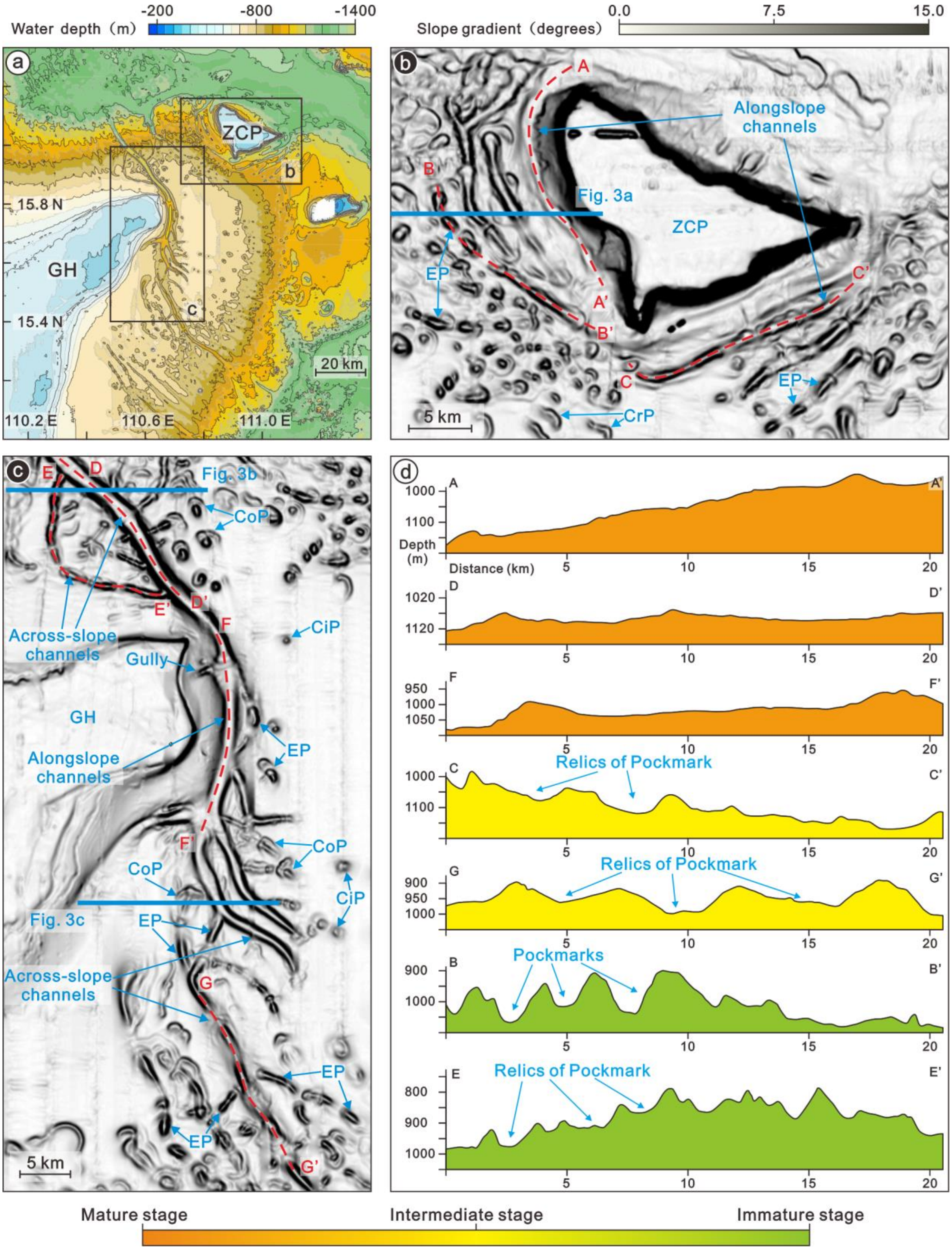

Figure 2. a) Bathymetric contour map revealing the distribution of submarine channels between the Guangle High (GH) and the Zhongjianbei Carbonate Platform (ZCP). b) and c) Slope gradient maps showing the morphology of submarine channels and pockmarks around the GH and ZCP. Red dashed lines indicate the thalwegs of the submarine channels depicted in the topographic profiles in (d). Solid blue lines indicate the location of the seismic profiles in Figure 3. CiP-Circular Pockmark; CoP-Comet Pockmark; CrP-Crescent Pockmark; EP-Elongated Pockmark. d) Topographic profiles highlighting the axial morphology of submarine channels and semi-connected pockmarks near the heads of discrete channels (e.g., B-B'). Green, yellow and orange colors indicate the channels that are immature, intermediate and mature in their evolution. Vertical axis stresses the variations in the depth of occurrence of the channel thalwegs. Detailed morphometric data for the submarine channels is given in Table S1.

5. Channel systems

The studied submarine channels can be classified into alongslope and across-slope channels based on their orientation and geometry (Figures 1b and 2). In addition, they have been defined as mature and immature channels based on: a) the roughness of their thalwegs, and b) the relative continuity of channel plane morphology (Figure 2, Table S1). In essence, mature channels reveal smoother thalwegs and a more continuous morphology when compared to immature channels (Figure 2).

5.1. Across-slope channels

Across-slope channels are perpendicular to the regional bathymetric slopes and chiefly located north and south of the GH (Figures 1b and 2c). As an example, a large across-slope channel (D-D' in Figures 2c and 2d), north of the GH (at ~16°N), is shown as a ~38 km long feature with a gentle thalweg dipping towards the NW (Figures 1b and 2c). As the most significant mature channel in the study area, channel D-D' has the smoothest thalweg, the largest average channel bankfull width and height, which are 2.6 km and 240 m, respectively (Figures 2c and 2d). Channel D-D' is connected to the alongslope channel F-F' at its southern end (Figure 2c).

Multiple immature channels and across-slope pockmark trains are connected to channel D-D' (Figure 2c). In the southwestern part of channel D-D', immature channel E-E' has a rough thalweg and is connected to channel D-D' at both its ends (Figures 2c and 2d). Channel E-E' is significantly shorter (~20 km) than channel D-D', and it is also narrower and shallower in its bankfull width (1.1 km in average) and height (94 m in average), respectively.

South of the GH, where the slope gradient is ~0.5°, several across-slope channels follow a SE orientation (Figures 1b and 2a). Channels are roughly parallel to each other and 30 to 50 km long (Figure 1b). They have rugged thalwegs and discontinuous morphologies (Figure 1b). These across-slope channels have bankfull widths from 1 to 1.5 km and bankfull heights between 50 and 200 m (Figures 1b and 2c). Importantly, the across-slope channel G-G' is in a zone with abundant isolated pockmarks and pockmark trains (Figures 1b and 2c). Southwest of channel G-G', the across-slope channels occur on the slope and remain ~15 km distant from the GH (Figure 1b). To the north of channel G-G', two across-slope channels of ~14 km and ~18 km long reveal a relatively flat thalweg and connect to the south end of the channel F-F' (Figure 2c). They are 1.5 km wide on average, and have a bankfull height of 50-150 m.

5.2. Alongslope channels

Alongslope channels are mainly observed along the south and west slopes of the ZCP and to the east of the GH (Figures 2b and 2c). To the east of the GH, an alongslope channel (F-F') is identified as a ~20 km long feature running parallel to the 800 m bathymetric contour (Figures 2a and 2c). Channel F-F' has an average bankfull width of 2.6 km and its bankfull height ranges from 150 to 180 m (Table S1). Channel F-F' has a smooth thalweg and two significant topographic highs (~50 m high) at both its ends (Figure 2d). These two highs occur at the confluences of channel F-F' with across-slope channels to the north and south (Figure 2c). A small channel with a sharp bend (~1.5 km wide, ~9 km long and with an average bankfull height of 120 m), and trains of elongated pockmarks (~1.3 km wide and ~90 m deep), join channel F-F' in its eastern part (Figures 2b and 3c).

Alongslope channels are the most significant features around the ZCP, being parallel to the platform slopes at a water depth between 1000 and 1200 m (Figures 1b and 2b). Here, the length of alongslope channels ranges from 10 to 25 km, with their bankfull width varying between 1 and 2.5 km. Their bankfull height ranges between 50 and 200 m. The channel closest to the ZCP (A-A') are the shallowest, with average channel bankfull heights of 73 m (Figure 1b and Table S1). These channels present elevations within their thalwegs that are more than 150 m high, with slope gradients of 0.5°- 0.9° (Figure 2d). Furthermore, the channels closer to the ZCP, such as A-A', have smoother thalwegs and more continuous plan-view morphologies when compared to more distant channels, i.e. B-B' and C-C' (Figures 2b and 2d). Several elongated pockmarks and alongslope pockmark trains occur along or parallel to these channels (Figure 2b).

5.3. Seismic architecture of channels and pockmarks

Seismic reflections are generally continuous and parallel between modern across-slope channels (e.g., D-D') and horizon T20 (Figures 3b and 3c). In contrast, seismic reflections beneath the modern alongslope channels (e.g., the channel next to A-A') are significantly truncated (Figure 3a). Chaotic strata with low amplitude are rarely identified in the channel-fill deposits of modern channel (Figure 3). Channel D-D' is remarkably wider, and with a greater bankfull height, when compared to the other channels imaged in seismic data (Figures 3 and S4). The inception of some channels, such as D-D', is recognized between horizons T20 and T30 (Figure 3), with a limited number of channels initiated below horizon T30 (Figures S4 and S6). Channel A-A' is a moat at the foot of the ZCP associated with a contourite drift, it shows a typical mounded shape with internal reflections dipping towards the bottom of channel A-A' (Figure 3a).

There are significant differences among the seismic cross-sections of across-slope and alongslope channels. Alongslope channels, such as the channel next to channel A-A', show distinctive truncations at their banks (Figure 3a). In contrast, across-slope channels, such as channel D-D' are usually located above paleo-channels with chaotic and high amplitude seismic reflections on their bases (Figs. 3b and S4). Seismic reflections on the banks of across-slope channels generally dip towards the channel thalweg (Figures 2b, 2c and S4). Fluid escape features are identified as convex or chaotic seismic reflections crossing particular seismic reflections (Figure 3). These fluid escape features are sourced from strata older than horizon T30, and truncate the seismic reflections above this same horizon (Figure 3). Most of them are connected to channels and pockmarks on the modern seafloor (Figures 3, S4, S5 and S6). Some paleo-pockmarks were buried after horizon T30, while some pockmarks at the modern seafloor show oblique migration since their inception (Figure 1d).

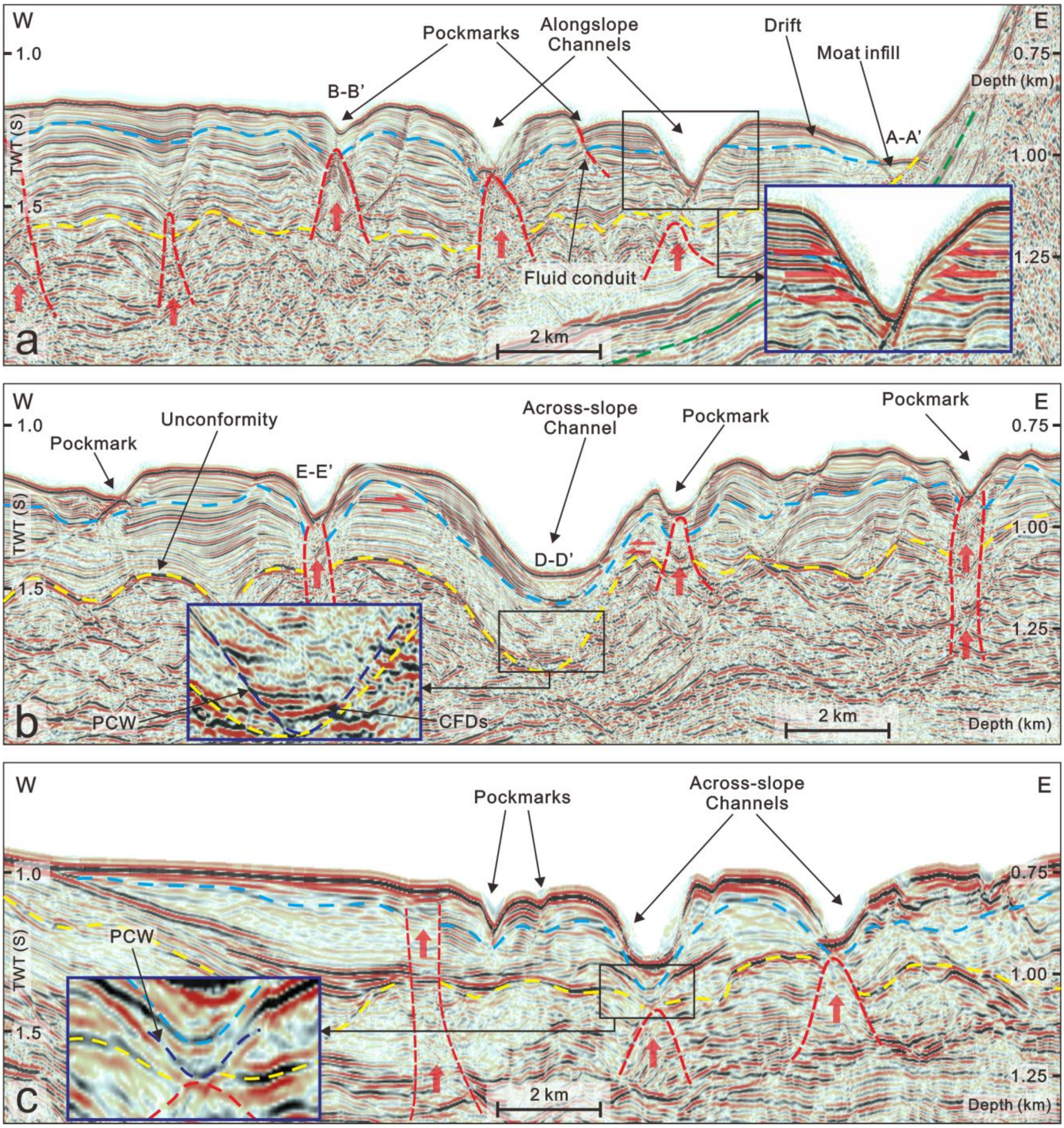

Figure 3. Seismic profiles (a-c) across submarine channels and seafloor pockmarks. Zoomed-in insets highlight the detailed geometry of past and present-day channels. Blue and yellow dashed lines mark the base of Quaternary (T20) and Pliocene (T30) strata, respectively. Fluid escape features are marked in the figure by red dashed lines and red vertical arrows. Red horizontal arrows in a) mark the presence of erosional truncations on the banks of alongslope channels. PCW: Paleo-channel Wall; CFDs:

Channel-fill Deposits. The location of the seismic profiles is shown in Figures 2b and 2c.

6. Discussion

6.1. Genesis of submarine channels and their relationship to pockmark trains

The studied submarine channels show variable orientations. Alongslope channels such as A-A’ and F-F’ run parallel to the slope contours, whereas across-slope channels (D-D’ and G-G’) developed perpendicularly to the slope topography (Figures 1b and 2). Previous studies have proposed that, in the study area, submarine channels comprise moats and furrows were formed by contour currents (Yin et al., 2021). However, some of the furrows and channels described in Yin et al. (2021) are perpendicular to the slope contours and, thus, unlikely to be associated with contour currents flowing alongslope. Therefore, other factors probably control their origin in the study area. Other oceanographic processes such as internal waves (e.g., internal tides) can flow transversely to the slope, forming intense near-seafloor currents and resuspending sediments, especially inside the largest canyons (Puig et al., 2013; 2014; Aslam et al., 2018). In the northern South China Sea, internal tides have been considered as a process responsible for downslope-migrating sand dunes (Ma et al., 2016). Although internal tides could, in part, contribute to the erosion of the interpreted channels, they are probably not the main factor controlling their origin in our study area, and they may be related to gravity processes.

Interactions between gravity processes and fluid escape in pockmarks can reshape the latter to form comet-shaped pockmarks oriented perpendicularly to the slope (Chen et al., 2019), and across-slope channels (Gay et al., 2006; Pilcher and Argent, 2007; Nakajima et al., 2014). Several pockmark trains are perpendicular to the slope gradient north and south of the GH, effectively comprising circular, comet-shaped and elongated pockmarks (Figure 1b). On the slopes surrounding the GH, active gas seepage brings deep, unlithified sediment to the seafloor through the pockmarks, while the GH comprises an active carbonate factory from where sediments are derived, contributing to the occurrence of gravity flows and slumps (Gay et al., 2006; Nakajima et al., 2014; Lu et al., 2017; Yang et al., 2021). Under the erosion of gravity currents on their adjacent slopes, circular pockmarks were reshaped to form elongated and comet-shaped pockmarks. Furthermore, pockmarks are not only scattered around the investigated channels, but also occur inside the channels themselves; hence, irregular depressions in channel thalwegs are the relics of reshaped pockmarks (e.g., G-G’ and E-E’ in Figure 2). Pre-existing pockmark trains affected by gravity currents probably contributed to the formation of across-slope channels on the slopes surrounding the GH. In the study area, the paleo-channels below modern across-slope channels commonly contain channel-fill deposits with chaotic and high amplitude seismic reflections onlapping the bases of paleo-channels (Figs. 3b and S4). These are typical seismic facies indicating the presence of gravity deposits (Figures. 3b and S4) (Wu et al., 2018).

Contrasting with across-slope channels, there are alongslope channels such as F-F', A-A' and C-C' that run parallel to the bathymetric contours (Figures 2b and 2c). They are likely formed by alongslope currents. Alongslope channels identified near the foot of the GH and ZCP (e.g., F-F' and A-A'; Figure 2b) are contourite moats and furrows associated with an isolated mounded drift recognized by Yin et al. (2021) (Figure 3a). They are thus related to the contour currents flowing along the GH and ZCP, which were strong enough to erode the seabed and generate erosional truncations on the banks of alongslope channels (Figures 2a, S4 and S6). Although average bottom currents are relatively weak in the western South China Sea, below 20 cm/s, they can be very variable and reach a maximum velocity close to 80 cm/s (Figure S9; Stow et al., 2013; Yang et al., 2019). These periods of intense circulation could be responsible for the observed seafloor erosion.

In addition, Andresen et al. (2008) and Kilhams et al. (2011) have suggested that bottom currents can induce the erosion of pockmarks, reshaping and coalescing them along the direction of bottom currents. When this process is maintained for a relatively long time, it results in the formation of alongslope channels, similarly to what is observed in the southwest and southeast flanks of the ZCP (Figures 1b and 2). Bottom current erosion in its broader sense is enhanced on their leeway side of pockmarks to form asymmetric and elongated features (Figure 2b; Masoumi et al., 2013). The elongated pockmarks are furtherly eroded and coalesce to form channels. In fact, relics of elongated pockmarks are found as asymmetric depressions in some of the channel thalwegs, e.g., in channel C-C' (Figure 2d).

6.2. Evolution of submarine channels in the western South China Sea

Micallef et al. (2014) first tested the concept of space-for-time substitution when reconstructing the evolution of submarine canyons and channel systems on continental margins. They suggested that, when the established model matches well with the morphological patterns interpreted on geophysical data, time can be substituted by space to reconstruct the evolution of canyons and channels. To illustrate channel development in the study area, we propose a space-for-time substitution model comprising three stages: a) a channel-inception stage, in which trains of pockmarks provide favorable pathways for eroding gravity flows and bottom currents, b) an immature stage, during which discrete pockmarks are elongated and coalesce to form immature channels with a rugged thalweg and a discontinuous morphology in plan-view, once again under the erosion of gravity flows or bottom currents, c) a mature stage, in which bottom currents and gravity flows are funneled through the channels to smooth their floor and banks (Figure 4). Therefore, under the erosion of gravity processes and bottom currents, pockmark trains gradually form immature channels to finally evolve into a complex system of across-slope and alongslope channels (Figure 4).

In the study area, Lu et al. (2017) proposed that the accumulation and dissociation of gas hydrates significantly contributed to the formation of pockmarks. In parallel, Gao et al. (2019) have suggested that pockmarks were formed by hydrothermal fluid flow induced by intensified hydrothermal activity occurring since the Pliocene. The oldest paleo-channel below channel D-D’ occurs between horizons T20 and T30, suggesting the Pliocene as the time of its inception (Figures 1d and 3). Channel D-D’ is one of the most mature in the study area and its stratigraphic position correlates with a period of enhanced hydrothermal activity in the Pliocene as identified in Gao et al. (2019). However, there are differences in the timing of inception of other channels, even when considering different reaches of the same channel. Some alongslope channels such as A-A’ have eroded horizon T20, indicating they are formed after the Pliocene (Figures 3a and S2). Other alongslope channels were identified under horizon T30, on the southeastern flank of ZCP, suggesting an earlier inception (Figure S6). According to the seismic data, the earliest time for channel inception in the study area can be traced to the Late Miocene.

Seismic reflections on the banks of channel D-D’, above horizon T20, are continuous and parallel, but seismic reflections between horizons T20 and T30 are truncated by paleo-channels or horizon T20, suggesting that erosive processes dominated during channel inception, with the resulting channels becoming filled in their mature stages (Figure 3b). Widespread immature channels such as E-E’, and pockmark trains such as B-B’, formed around mature channels also show that the investigated system of channels is still evolving (Figure 2). Abundant truncations on the banks of immature channels suggest that erosive processes still dominate their development (Figure 3). This means that present-day immature channels can still evolve into mature features if gravity processes and bottom currents keep eroding the seafloor pockmarks mapped in this work (Figure 4).

Channel evolution was significantly influenced by seafloor topography, which predominantly controlled the dynamics of ocean currents. Changes in slope gradient can not only determine the formation of channels, but also control the transition between erosional and aggradational processes in them (Micallef and Mountjoy, 2011). Slope gradients differ in the north, south and east of the GH; hence the steepest slope (~0.8°) north of the GH led to the formation of channel D-D’, which is the widest, more deeply incised of all channels. Mature and immature channels also formed on the slope to the south of the GH, which records a moderate gradient of ~0.5° (Figures 2 and 4). The slope to the east of the GH does not present any across-slope channels, probably because it is relatively gentle (<0.3°) and, therefore, relatively stable and less likely to be affected by gravity processes (Figures 2 and 4). In addition, it is known that bathymetric obstacles influence the dynamics of bottom currents and control the formation of alongslope channels (Hernández-Molina et al., 2006; Yin et al., 2021). Thus, alongslope channels were commonly formed around the GH and ZCP (Figures 2).

Mulder et al. (2017) demonstrated that sediment supplied by channels (or canyons) onto deep-water depocenters can originate from topographic highs instead of a point source. One gully located on the eastern slope of the GH is connected to channel F-F’ in a zone with a topographic high in the thalweg (Figure 2c). This zone may also contain gravity deposits transported from the platform but, unfortunately, no seismic or sediment core data were available to confirm such an assumption. Furthermore, Wu et al. (2016) revealed a similar Early Pliocene paleo-topography to the modern seafloor topography, and considered it to have an important morphological control on the development of channel systems.

Compared to other well-studied channels in the South China Sea (Chen et al., 2020), the channel system investigated in this work is characterized by its complicated morphology and the effect of multiple mechanisms in its development. Hence, the recognition of a system of across-slope and alongslope channels, initiated from pockmarks, and influenced by seafloor topography, has significant implications to the current understanding of how submarine channels are initiated on continental margins across the world.

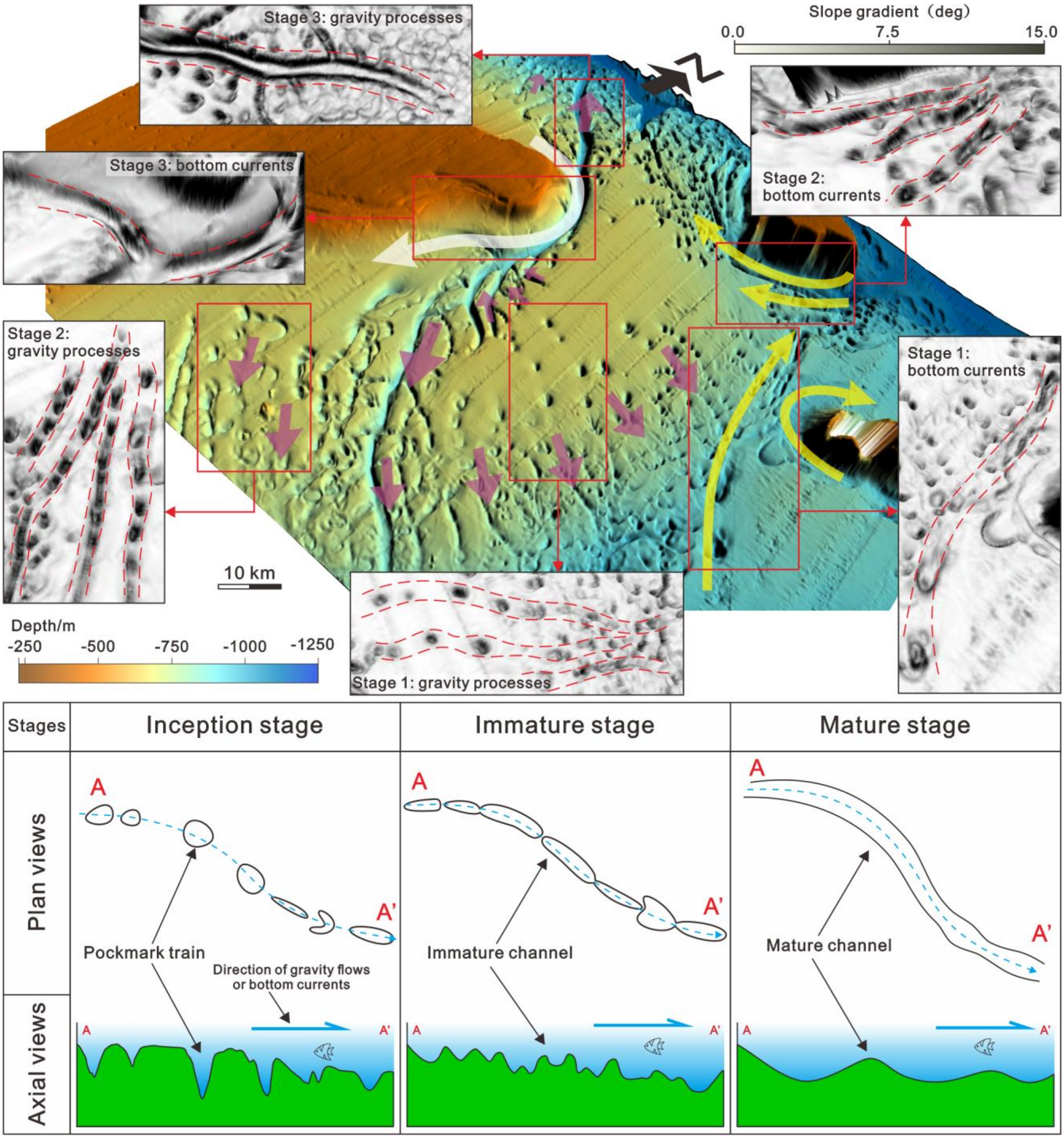

Figure 4. Schematic diagrams, combined with a three-dimensional morphological map of the study area, summarizing the time-step evolution of channels around the interpreted pockmark field. Stage 1: submarine channel inception is controlled by a pockmark train; Stage 2: under the effect of gravity processes and bottom currents, discrete pockmarks are eroded and coalesce to form an immature channel; Stage 3: gravity processes and bottom currents continue to erode the immature channel, which subsequently evolves into a mature channel presenting a smooth, continuous thalweg. The purple arrows indicate the direction of gravity processes. The white and yellow

arrows indicate the pathways of bottom currents at water depths of ~800 m and ~1000 m, respectively.

7. Conclusions

High-resolution multibeam bathymetry and two-dimensional seismic data enabled us to investigate the morphology of a complex system of channels in the western South China Sea, plus its genesis and evolution. The main conclusions of this study are as follows:

(1) The studied channel system comprises a large number of across-slope and alongslope channels found within a giant pockmark field, which covers an area of more than 9,000 km^2 at a water depth of 700-1200 m.

(2) The channels analyzed in this study are formed by the incision of gravity processes and bottom currents on seafloor pockmarks, particularly on those arranged as pockmark trains.

(3) Based on the space-for-time substitution concept, the evolution of the channels can be summarized in three stages: Stage 1, in which the inception of the studied channels coincided with the erosion of pockmark trains; Stage 2, in which pockmark trains were eroded by gravity flows and bottom currents to form immature channels; Stage 3, during which immature channels evolved into mature channels, with a flatter channel floor, under the effect of continuing erosion.

(4) The studied channel system was firstly initiated in the Late Miocene, and is still developing at present. Discrete channels in this system were formed at different times, and their evolution has been significantly controlled by an ever-evolving seafloor topography.

Acknowledgments

This work was financially supported by Key Special Project for Introduced Talents Team of Southern Marine Science and Engineering Guangdong Laboratory (Guangzhou) (GML2019ZD0104), Guangdong Basic and Applied Basic Research Foundation (2020B1515020016) and National Scientific Foundation of China (41876054). Dr. Wei Li is funded by CAS Pioneer Hundred Talents Program (Y8SL011001). We thank China National Petroleum Corporation (CNPC) and Guangzhou Marine Geological Survey (GMGS) for their permission to release the data. The multibeam bathymetric/seismic reflection data may be requested from CNPC/GMGS. We thank for the scholarship provided by University of Chinese Academy of Sciences (UCAS) to support the research stay of Mr. Kaiqi Yu at the University of Bremen. We thank Chief Editor Prof. Dr. Harihar Rajaram and the reviewers Dr. Michele Rebesco, Dr. Walter Barnhardt and an anonymous reviewer for their constructive comments that helped us improve our manuscript.

Data Availability Statement

The multibeam bathymetric data for this research are sourced from Lu et al. (2018) at https://doi.org/10.1190/INT-2017-0222.1, The seismic data used are freely available at the repository https://zenodo.org/record/5045344#.YNxV6OgzZhE.

References

Allen, P. A. (2017), Sediment routing systems: The fate of sediment from source to sink, *Cambridge University Press*, pp.18-19.

Andresen, K. J., Huuse, M., & Clausen, O. R. (2008), Morphology and distribution of Oligocene and Miocene pockmarks in the Danish North Sea - implications for bottom current activity and fluid migration. *Basin Research*, **20**(3), 445-466. doi: 10.1111/j.1365-2117.2008. 00362.x

Aslam, T., Hall, R. A., & Dye., S. R. (2018), Internal tides in a dendritic submarine canyon. *Progress in Oceanography*, **169**, 20-32. doi: https://doi.org/10.1016/j.pocean.2017.10.005

Astakhov, A. S. (2004a), Grain size composition of bottom sediments from East Asian marginal seas, core Ast-87063, edited, PANGAEA.

Astakhov, A. S. (2004b), Grain size composition of bottom sediments from East Asian marginal seas, core Ast-87061, edited, PANGAEA.

Chen, H., Xie, X., Mao, K., He, Y., Su, M., & Zhang, W. (2020), Depositional Characteristics and Formation Mechanisms of Deep-Water Canyon Systems along the Northern South China Sea Margin. *Journal of Earth Science*, **31**(4), 808-819. doi: https://doi.org/10.1007/s125 83-020-1284-z

Chen, TT., Paull, C. K., Liu, CS., Klaucke, I., Hsu, HH., Su, CC., Gwiazda, R., & Caress., D. W. (2019), Discovery of numerous pingos and comet-shaped depressions offshore southwestern Taiwan. *Geo-Marine Letters*, **40**(4), 407-421. doi: https://doi.org/10.1007/s00367-019-00577-z

Dandapath, S., Chakraborty, B., Karisiddaiah, S. M., Menezes, A., Ranade, G., Fernandes, W., ... & Raju, K. P. (2010), Morphology of pockmarks along the western continental margin of India: Employing multibeam bathymetry and backscatter data. *Marine and Petroleum Geology*, **27**(10), 2107-2117. doi: 10.1016/j.marpetgeo.2010.09.005

de Leeuw, J., Eggenhuisen, J. T., & Cartigny, M. J. (2016), Morphodynamics of submarine channel inception revealed by new experimental approach. *Nature communications*, **7**(1), 1-7. doi: 10.1038/ncomms10886

Fildani, A., Hubbard, S. M., Covault, J. A., Maier, K. L., Romans, B. W., Traer, M., & Rowland, J. C. (2013), Erosion at inception of deep-sea channels. *Marine and Petroleum Geology*, **41**, 48-61. doi: 10.1016/j.marpetgeo.2012.03.006

Gao, J., Bangs, N., Wu, S., Cai, G., Han, S., Ma, B., ... & Wang, D. (2019), Post-seafloor spreading magmatism and associated magmatic hydrothermal systems in the

Xisha uplift region, northwestern South China Sea. *Basin Research*, **31**(4), 688-708. doi: 10.1111/bre.12338

García, M., Hernández-Molina, F. J., Llave, E., Stow, D. A. V., León, R., Fernández-Puga, M. C., ... & Somoza, L. (2009), Contourite erosive features caused by the Mediterranean Outflow Water in the Gulf of Cadiz: Quaternary tectonic and oceanographic implications. *Marine Geology*, **257**(1-4), 24-40. doi: 10.1016/j.margeo.2008.10.009

Gay, A., Lopez, M., Cochonat, P., Séranne, M., Levaché, D., & Sermondadaz, G. (2006), Isolated seafloor pockmarks linked to BSRs, fluid chimneys, polygonal faults and stacked Oligocene–Miocene turbiditic palaeochannels in the Lower Congo Basin. *Marine Geology*, **226**(1-2), 25-40. doi: 10.1016/j.margeo.2005.09.018

Gay, A., Lopez, M., Berndt, C., & Seranne, M. (2007), Geological controls on focused fluid flow associated with seafloor seeps in the Lower Congo Basin. *Marine Geology*, **244**(1-4), 68-92. doi: 10.1016/j.margeo.2007.06.003

Hansen, L., Janocko, M., Kane, I., & Kneller, B. (2017), Submarine channel evolution, terrace development, and preservation of intra-channel thin-bedded turbidites: Mahin and Avon channels, offshore Nigeria. *Marine Geology*, **383**, 146-167. doi: 10.1016/j.margeo.2016.11.011

Hernández-Molina, J., Llave, E., Somoza, L., Fernández-Puga, M. C., Maestro, A., León, R., ... & Gardner, J. (2003), Looking for clues to paleoceanographic imprints: a diagnosis of the Gulf of Cadiz contourite depositional systems. *Geology*, **31**(1), 19-22. https://doi.org/10.1130/0091-7613(2003)031<0019:LFCTPI>2.0.CO;2

Hernández-Molina, F. J., Larter, R. D., Rebesco, M., & Maldonado, A. (2006), Miocene reversal of bottom water flow along the Pacific Margin of the Antarctic Peninsula: stratigraphic evidence from a contourite sedimentary tail. *Marine Geology*, **228**(1-4), 93-116. doi: 0.1016/j.margeo.2005.12.010

Hillman, J. I., Klaucke, I., Pecher, I. A., Gorman, A. R., Schneider von Deimling, J., & Bialas, J. (2018), The influence of submarine currents associated with the Subtropical Front upon seafloor depression morphologies on the eastern passive margin of South Island, New Zealand. *New Zealand Journal of Geology and Geophysics*, **61**(1), 112-125. doi: 10.1080/00288306.2018.1434801

Hovland, M., Gardner, J. V., & Judd, A. G. (2002), The significance of pockmarks to understanding fluid flow processes and geohazards. *Geofluids*, **2**(2), 127-136. doi: 10.1046/j.1468-8123.2002. 00028.x

Kilhams, B., McArthur, A., Huuse, M., Ita, E., & Hartley, A. (2011), Enigmatic large-scale furrows of Miocene to Pliocene age from the central North Sea: current-scoured pockmarks. *Geo-Marine Letters*, **31**(5), 437-449. doi: 10.1007/s00367-011-0235-1

Lemay, M., Grimaud, J. L., Cojan, I., Rivoirard, J., & Ors, F. (2020), Geomorphic variability of submarine channelized systems along continental margins: Comparison with fluvial meandering channels. *Marine and Petroleum Geology*, **115**. doi: 10.1016/j.marpetgeo.2020.104295

León, R., Somoza, L., Medialdea, T., Hernández-Molina, F. J., Vázquez, J. T., Díaz-del-Rio, V., & González, F. J. (2010), Pockmarks, collapses and blind valleys in the Gulf of Cádiz. *Geo-Marine Letters*, **30**(3-4), 231-247. doi: 10.1007/s00367-009-0169-z

Li, C. F., Xu, X., Lin, J., Sun, Z., Zhu, J., Yao, Y., ... & Zhang, G. L. (2014), Ages and magnetic structures of the South China Sea constrained by deep tow magnetic surveys and IODP Expedition 349. *Geochemistry, Geophysics, Geosystems*, **15**(12), 4958-4983. doi: https://doi.org/10.1002/2014GC005567

Li, W., Alves, T. M., Wu, S., Völker, D., Zhao, F., Mi, L., & Kopf, A. (2015), Recurrent slope failure and submarine channel incision as key factors controlling reservoir potential in the South China Sea (Qiongdongnan Basin, South Hainan Island). *Marine and Petroleum Geology*, **64**, 17-30. doi:10.1002/ 2014GC005567.

Liu, Q., Kaneko, A., & Jilan, S. (2008), Recent progress in studies of the South China Sea circulation. *Journal of Oceanography*, **64**(5), 753-762. doi: 10.1007/s10872-008-0063-8

Lu, Y., Li, W., Wu, S., Cronin, B. T., Lyu, F., Wang, B., ... & Ma, B. (2018), Morphology, architecture, and evolutionary processes of the Zhongjian Canyon between two carbonate platforms, South China Sea. *Interpretation*, **6**(4), SO1-SO15. doi: https://doi.org/10.1190/INT-2017-0222.1

Lu, Y., Luan, X., Lyu, F., Wang, B., Yang, Z., Yang, T., & Yao, G. (2017), Seismic evidence and formation mechanism of gas hydrates in the Zhongjiannan Basin, Western margin of the South China Sea. *Marine and Petroleum Geology*, **84**, 274-288. doi: 10.1016/j.marpetgeo.2017.04.005

Ma, X., Yan, J., Hou, Y., Lin, F., & Zheng, X. (2016), Footprints of obliquely incident internal solitary waves and internal tides near the shelf break in the northern South China Sea. *Journal of Geophysical Research: Oceans*, **121**(12), 8706-8719. doi: 10.1002/2016JC012009

Masoumi, S., Reuning, L., Back, S., Sandrin, A., & Kukla, P. A. (2014), Buried pockmarks on the Top Chalk surface of the Danish North Sea and their potential significance for interpreting palaeocirculation patterns. *International Journal of Earth Sciences*, **103**(2), 563-578. doi: 10.1007/s00531-013-0977-2

Micallef, A., & Mountjoy, J. J. (2011), A topographic signature of a hydrodynamic origin for submarine gullies. *Geology*, **39**(2), 115-118. https://doi.org/10.1130/G31475.1

Micallef, A., Ribó, M., Canals, M., Puig, P., Lastras, G., & Tubau, X. (2014), Space-for-time substitution and the evolution of a submarine canyon–channel system in a passive progradational margin. *Geomorphology*, **221**, 34-50. doi: 10.1016/j.geomorph.2014.06.008

Miramontes, E., Jouet, G., Thereau, E., Bruno, M., Penven, P., Guerin, C., ... & Cattaneo, A. (2020), The impact of internal waves on upper continental slopes: insights from the Mozambican margin (SW Indian Ocean). *Earth Surface Processes and Landforms,* **45**(6), 1469-1482. doi: 10.1002/esp.4818

Miramontes, E., P. Garreau, M. Caillaud, G. Jouet, R. Pellen, F. J. Hernández-Molina, M. A. Clare, & A. Cattaneo (2019), Contourite distribution and bottom currents in the NW Mediterranean Sea: Coupling seafloor geomorphology and hydrodynamic modelling. *Geomorphology*, **333**, 43-60. doi: 10.1016/j.geomorph.2019.02.030

Miramontes, E., Thiéblemont, A., Babonneau, N., Penven, P., Raisson, F., Droz, L., ... & Jouet, G. (2021), Contourite and mixed turbidite-contourite systems in the Mozambique Channel (SW Indian Ocean): Link between geometry, sediment characteristics and modelled bottom currents. *Marine Geology*, **437**, 106502. doi: https://doi.org/10.1016/j.margeo.2021.106502

Mulder, T., Gillet, H., Hanquiez, V., Ducassou, E., Fauquembergue, K., Principaud, M., ... & Seibert, C. (2018). Carbonate slope morphology revealing a giant submarine canyon (Little Bahama Bank, Bahamas). *Geology*, **46**(1), 31-34. doi: https://doi.org/10.1130/G39527.1

Nakajima, T., Kakuwa, Y., Yasudomi, Y., Itaki, T., Motoyama, I., Tomiyama, T., ... & Matsumoto, R. (2014), Formation of pockmarks and submarine canyons associated with dissociation of gas hydrates on the Joetsu Knoll, eastern margin of the Sea of Japan. *Journal of Asian Earth Sciences*, **90**, 228-242. doi: https://doi.org/10.1016/j.jseaes.2013.10.011

Pilcher, R., & Argent, J. (2007), Mega-pockmarks and linear pockmark trains on the West African continental margn. *Marine Geology*, **244**(1-4), 15-32. doi: 10.1016/j.margeo.2007.05.002

Puig, P., Palanques, A., & Martín, J. (2014), Contemporary sediment-transport processes in submarine canyons. *Annual Review of Marine Science*, **6**, 53-77. doi: 10.1146/annurev-marine-010213-135037

Puig, P., Greenan, B. J., Li, M. Z., Prescott, R. H., & Piper, D. J. (2013), Sediment transport processes at the head of Halibut Canyon, eastern Canada margin: An interplay between internal tides and dense shelf-water cascading. *Marine Geology*, **341**, 14-28. doi:10.1016/j.margeo.2013.05.004

Quan, Q., & Xue, H. (2018), Layered model and insights into the vertical coupling of the South China Sea circulation in the upper and middle layers. *Ocean Modelling*, **129**, 75-92. doi: 10.1016/j.ocemod.2018.06.006

Rebesco, M., Hernández-Molina, F. J., Van Rooij, D., & Wåhlin, A. (2014), Contourites and associated sediments controlled by deep-water circulation processes: State-of-the-art and future considerations. *Marine Geology*, **352**, 111-154. doi: 10.1016/j.margeo.2014.03.011

Stow, D. A. V., Hernández-Molina, F. J., Llave, E., Bruno, M., García, M., del Rio, V. D., ... & Brackenridge, R. E. (2013), The Cadiz Contourite Channel: Sandy contourites, bedforms and dynamic current interaction. *Marine Geology*, **343**, 99-114. doi: 10.1016/j.margeo.2013.06.013

Wu, S., Zhang, X., Yang, Z., Wu, T., Gao, J., & Wang, D. (2016), Spatial and temporal evolution of Cenozoic carbonate platforms on the continental margins of the South China Sea: Response to opening of the ocean basin. *Interpretation*, **4**(3), SP1-SP19. doi: https://doi.org/10.1190/INT-2015-0162.1

Wu, W., Li, Q., Yu, J., Lin, C., Li, D., & Yang, T. (2018), The Central Canyon depositional patterns and filling process in east of Lingshui Depression, Qiongdongnan Basin, northern South China Sea. *Geological Journal*, **53**(6), 3064-3081. doi: https://doi.org/10.1002/gj.3143

Yang, Yuanzheng., Xu. C., Li. S., & He. Y. (2019), Ship-mounted ADCP data for ocean currents in the South China Sea (2009–2012). doi: 10.11922/csdata.2019.0006.zh

Yang, Z., Li, X., Huang, L., Wang, L., Wu, S., & Zhang, X. (2021), Development of the Miocene Guangle Carbonate Platform in the South China Sea: Architecture and Controlling Factors. *Acta Geologica Sinica - English Edition*, **95**(1), 177-191. doi: 10.1111/1755-6724.14639

Yin, S., Hernández-Molina, F. J., Lin, L., Chen, J., Ding, W., & Li, J. (2021), Isolation of the South China Sea from the North Pacific Subtropical Gyre since the latest Miocene due to formation of the Luzon Strait. *Scientific Reports*, **11**(1), 1562. doi: 10.1111/1755-6724.14639

Zhou, D., Ru, K., & Chen, H. Z. (1995), Kinematics of Cenozoic extension on the South China Sea continental margin and its implications for the tectonic evolution of the region. *Tectonophysics*, **251**(1-4), 161-177. doi: 10.1016/0040-1951(95)00018-6

Zhu, M., Graham, S., Pang, X., & McHargue, T. (2010), Characteristics of migrating submarine canyons from the middle Miocene to present: Implications for paleoceanographic circulation, northern South China Sea. *Marine and Petroleum Geology*, **27**(1), 307-319. doi: 10.1016/j.marpetgeo.2009.05.005

Geophysical Research Letters

Supporting information for

Incision of submarine channels over pockmark trains in the South China Sea

Kaiqi Yu [1, 2, 3], Elda Miramontes [4, 5], Tiago M. Alves [6], Wei Li [1, 2, 3 *], Linlin Liang [3, 7], Shuang Li [1, 2, 3], Wenhuan Zhan[1, 2, 3], Shiguo Wu [3, 8]

[1]Key Laboratory of Ocean and Marginal Sea Geology, South China Sea Institute of Oceanology, Innovation Academy of South China Sea Ecology and Environmental Engineering, Chinese Academy of Sciences, Guangzhou 510301, China.

[2]Southern Marine Science and Engineering Guangdong Laboratory (Guangzhou), Guangzhou 511458, China.

[3]University of Chinese Academy of Sciences, Beijing 100049, China.

[4]Faculty of Geosciences, University of Bremen, Bremen 28359, Germany.

[5]MARUM-Center for Marine Environmental Sciences, University of Bremen, Bremen, 28359, Germany.

[6]3D Seismic Laboratory,. School of Earth and Ocean Environmental Sciences, Cardiff University, Main Building, Park Place, Cardiff, CF10 3AT, United Kingdom.

[7]State Key Laboratory of Tropical Oceanography, South China Sea Institute of Oceanology, Chinese Academy of Sciences, Guangzhou, China.

[8]Institute of Deep-sea Science and Engineering, Chinese Academy of Sciences, Sanya, 572000, China

*Corresponding authors: Dr. Wei Li (wli@scsio.ac.cn)

Contents

Introduction

The uninterpreted seismic profiles (Figures S1 and S2) in Figures 1c and 3 are provided as supporting information to this work. They show details of the seismic architecture of investigated channels. Also shown a map with the location of all available seismic data interpreted in this study (Figure S3). Eight supplementary seismic profiles are provided for a more comprehensive analysis of pockmarks, alongslope and across-slope channels (Figures S4-S6). These seismic profiles highlight morphological differences among alongslope and across-slope channels. Diagrams explaining how channels and pockmarks were measured are provided in Figures S7 and S8. The speed profiles of ocean currents in western South China Sea are provided in Figure S9. Finally, Table S1 provides morphological details of the alongslope and across-slope channels highlighted in Figure 2.

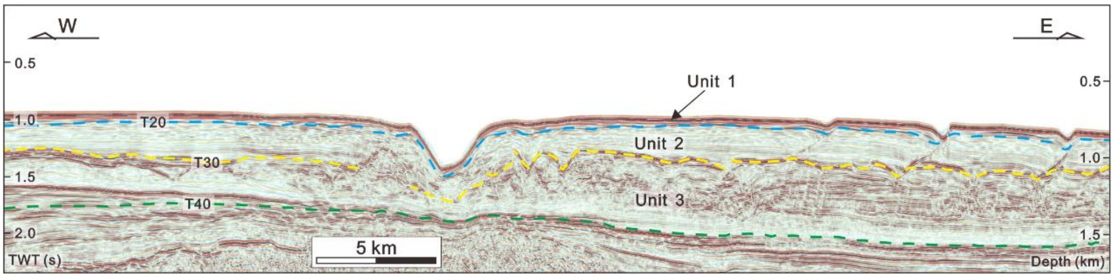

Figure S1. Interpretation of the seismic profile shown in Figure 1c. This study focuses on shallow strata in the western South China Sea, which are subdivided into three units: Unit 1 (Quaternary); Unit 2 (Pliocene) and Unit 3 (Late Miocene). The bases of these seismic-stratigraphic units correlate with seismic horizons T20, T30 and T40, respectively. The amplitude and continuity of seismic reflections show significant differences when comparing near-seafloor strata to the deeper units imaged in seismic data.

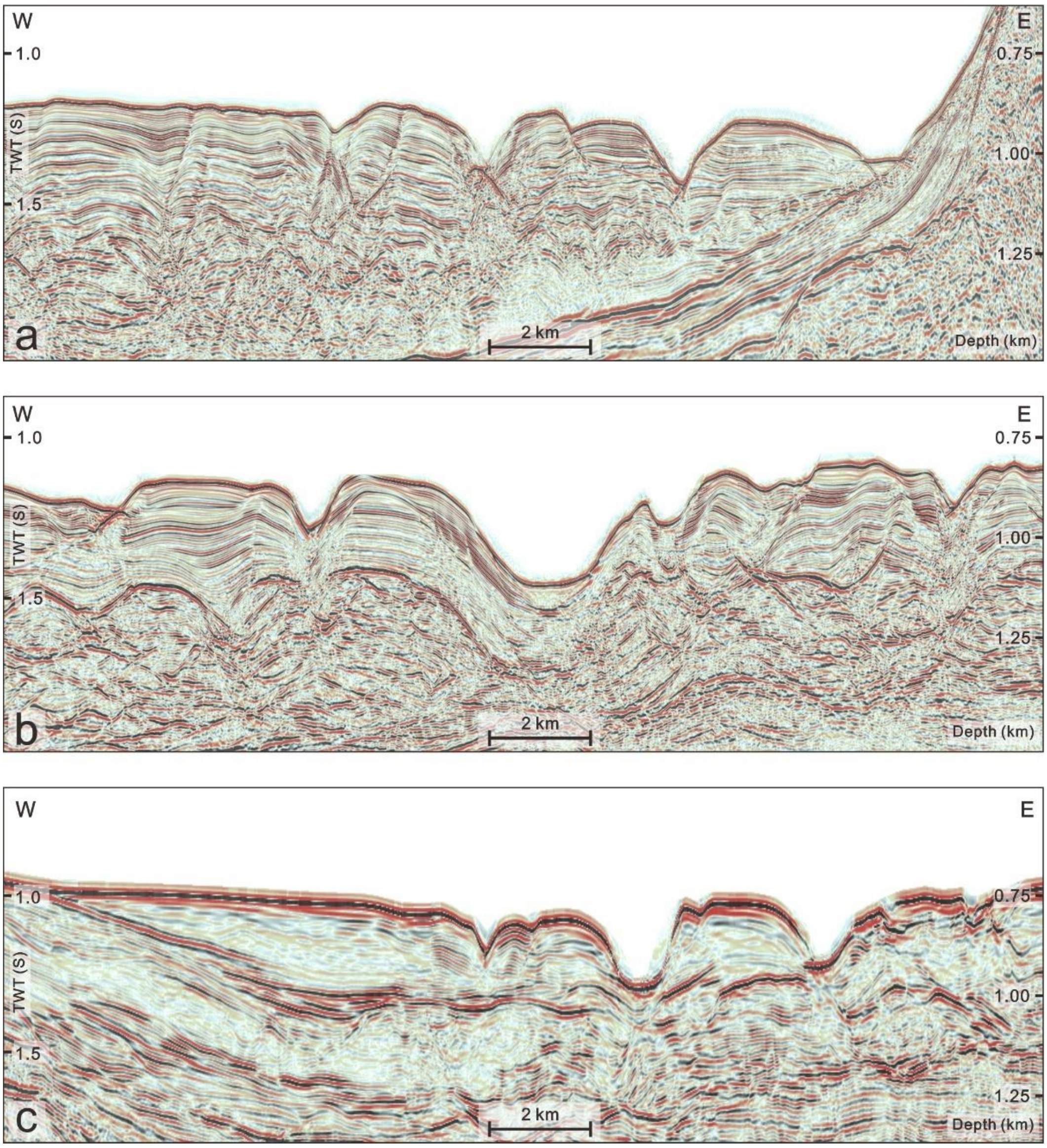

Figure S2. Uninterpreted versions of the seismic profiles shown in Figure 3. Seismic facies in the figure are markedly variable at depth. The seismic reflections close to the seafloor are parallel and continuous, but chaotic when moving deeper into the imaged succession.

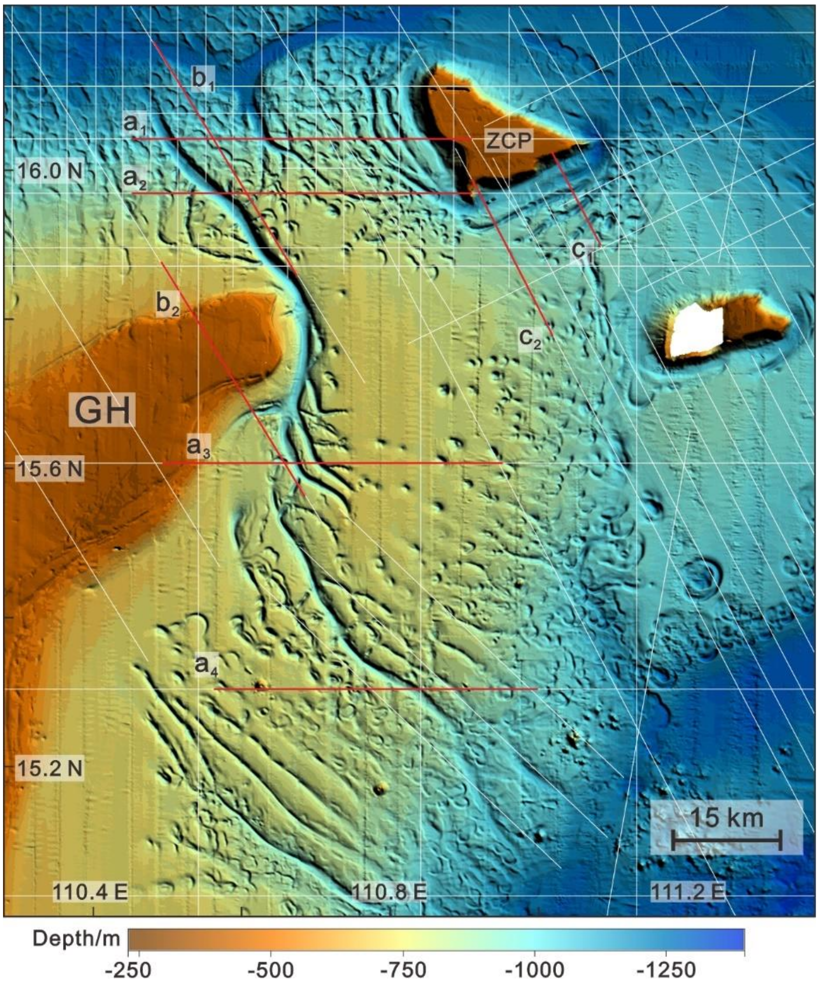

Figure S3. Bathymetric map of the study area highlighting the locations of the seismic profiles interpreted in this study (see white solid lines). The supplementary seismic profiles provided are labelled and shown by the red solid lines.

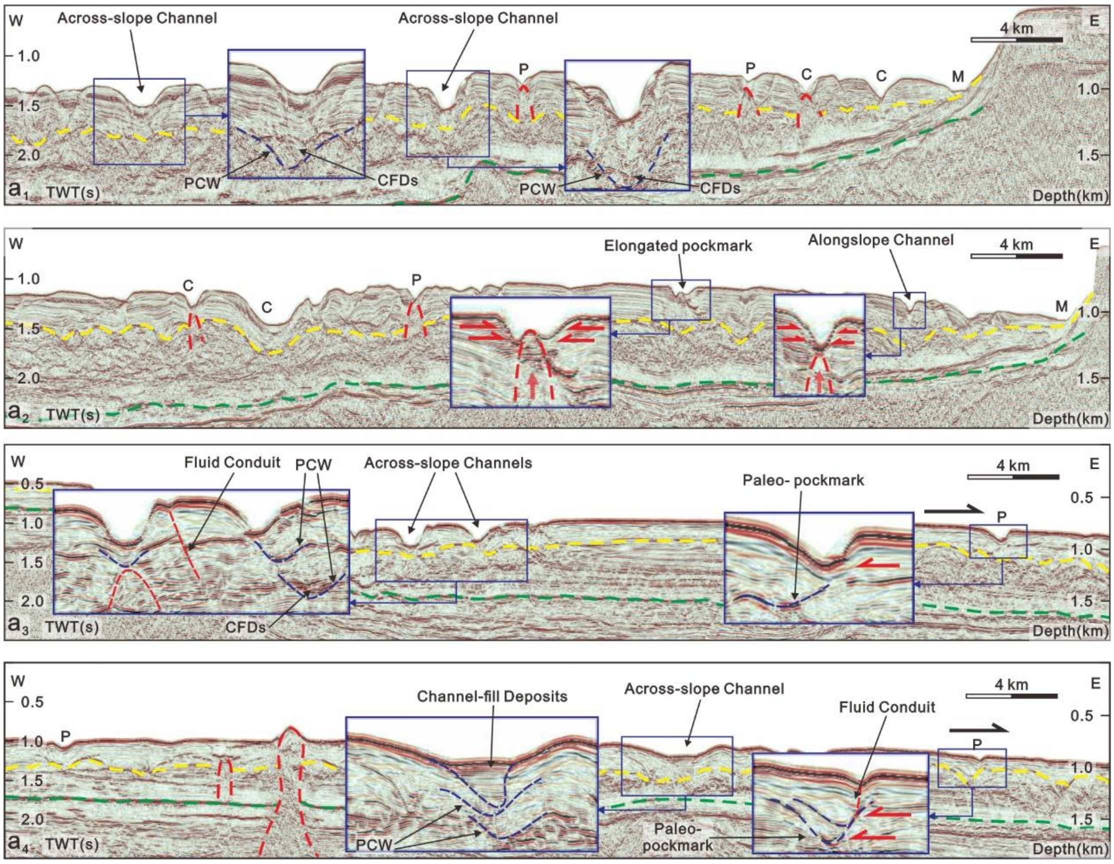

Figure S4. W-E seismic profiles (a_1, a_2, a_3 and a_4) highlighting the main morphological differences among across-slope and alongslope channels. The location of the four seismic profiles is shown in Figure S3. Yellow and green dashed lines indicate the bases of Pliocene (T30) and Late Miocene (T40) strata. The red dashed lines highlighting the presence of fluid escape features in the study area. Black horizontal arrows point out to the downslope direction. P: Pockmark; C: Channel; M: Moat; PCW: Paleo-channel wall; CFDs: Channel-fill Deposits; Zoomed-in insets show details of channels and pockmarks.

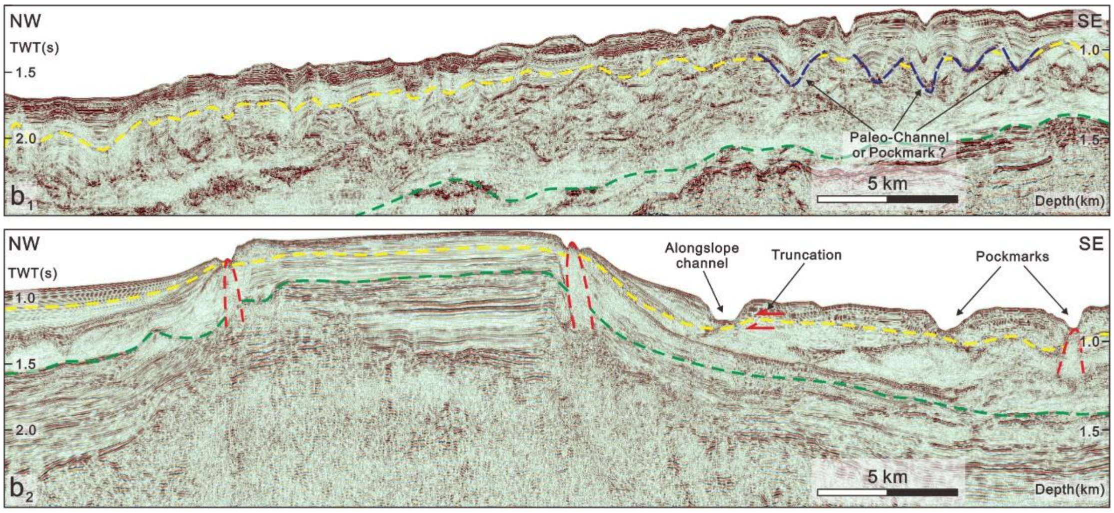

Figure S5. NW-SE seismic profiles revealing the seismic stratigraphy across the Guangle High (GH) and along the channel D-D' (shown in Figure 2c). The yellow and green dashed lines indicate the bases of Pliocene (T30) and Late Miocene (T40) strata. The red dashed lines highlight the presence of fluid escape features. Many paleo-channels (or paleo-pockmarks) are identified in the upper reaches of channel D-D', and truncate horizon T30 (Pliocene). The flanks of the GH are eroded by alongslope channels, as indicated by the erosional truncations shown in the seismic profile. See Figure S3 for the location of the two seismic profiles.

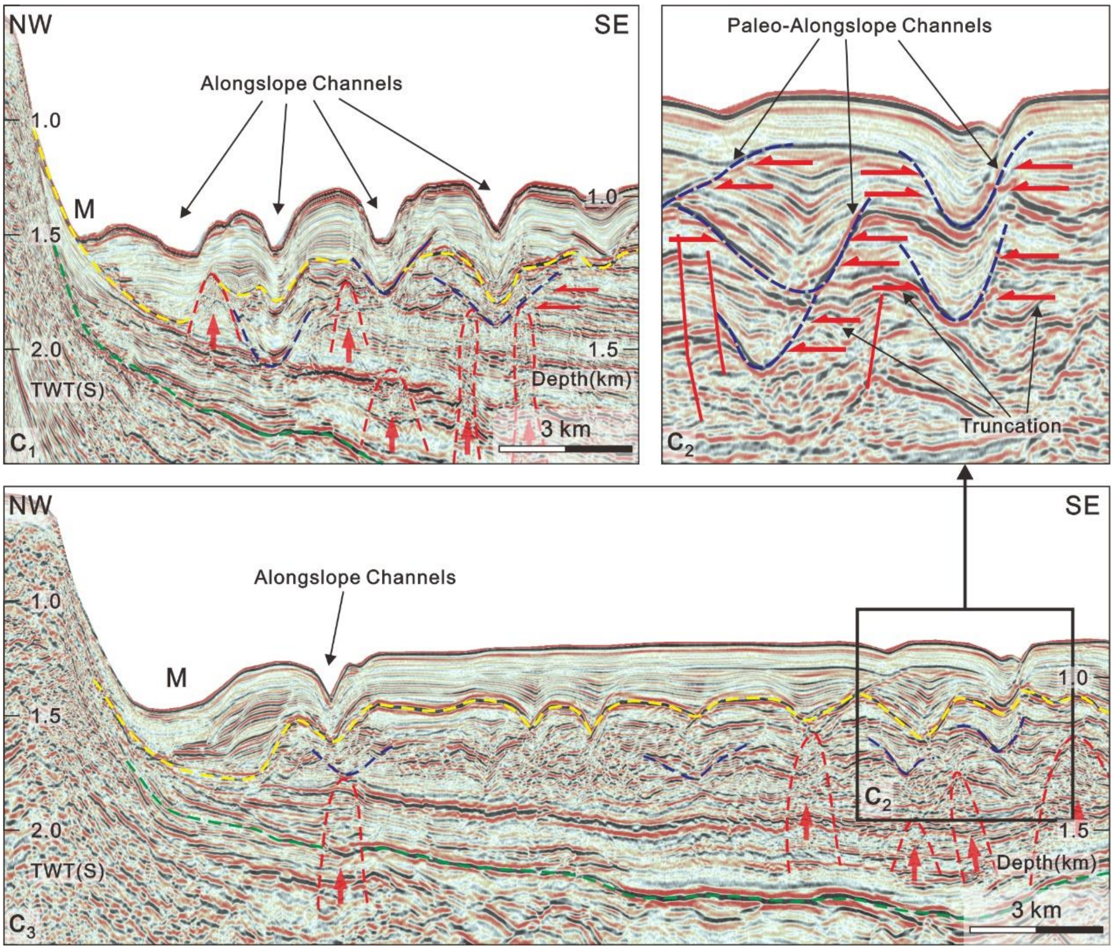

Figure S6. Seismic profiles oriented perpendicularly to the southeastern slope of the Zhongjianbei Carbonate Platform (ZCP). They highlight the cross-section morphology of the alongslope channels that are parallel to the slopes flanking the ZCP. The zoomed-in inset highlights the morphology of older alongslope channels. The bases of Pliocene (T30) and Late Miocene (T40) strata are indicated by the yellow and green dashed lines. Many paleo-channels and paleo-pockmarks (highlighted by the dark blue dashed lines) are identified below the modern channels, modern pockmarks and the seafloor. Older alongslope channels show erosional truncation on their flanks as indicated by the horizontal red arrows. Fluid escape features (shown as red dashed lines) originate from strata under horizon T30 or T40, revealing a close relationship with the channels and pockmarks above. M-moat. The location of the seismic profiles is shown in Figure S3.

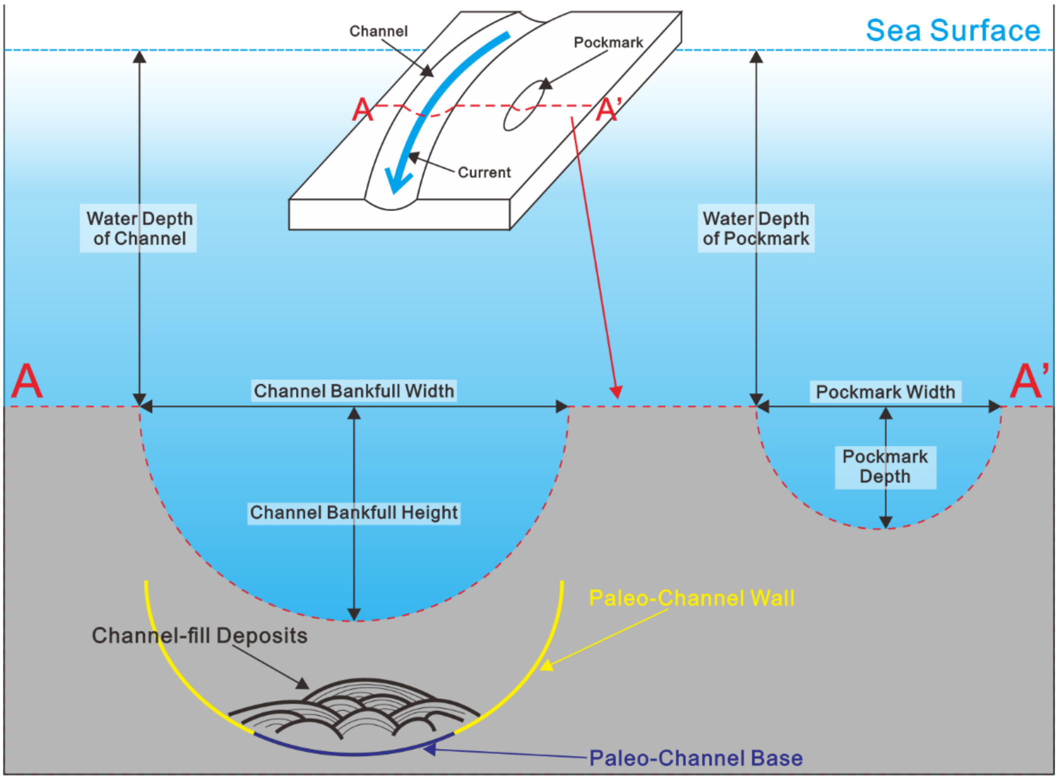

Figure S7. Diagram summarizing the definitions of water depth of channel and pockmark, channel bankfull width and height, pockmark depth and width, paleo-channel wall and base, channel-fill deposits used in this work.

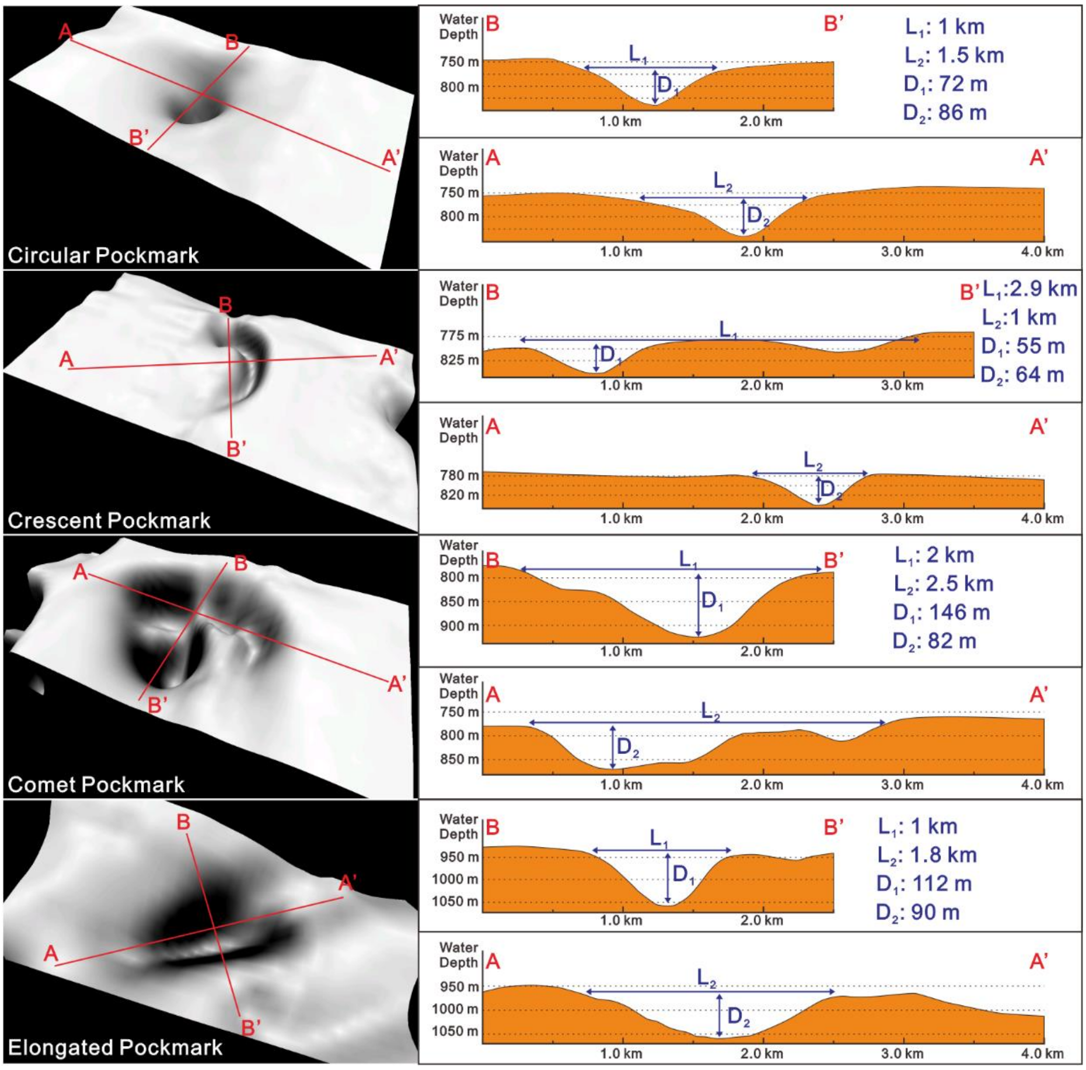

Figure S8. Morphological data for circular, crescent, comet and elongated pockmarks in the study area.

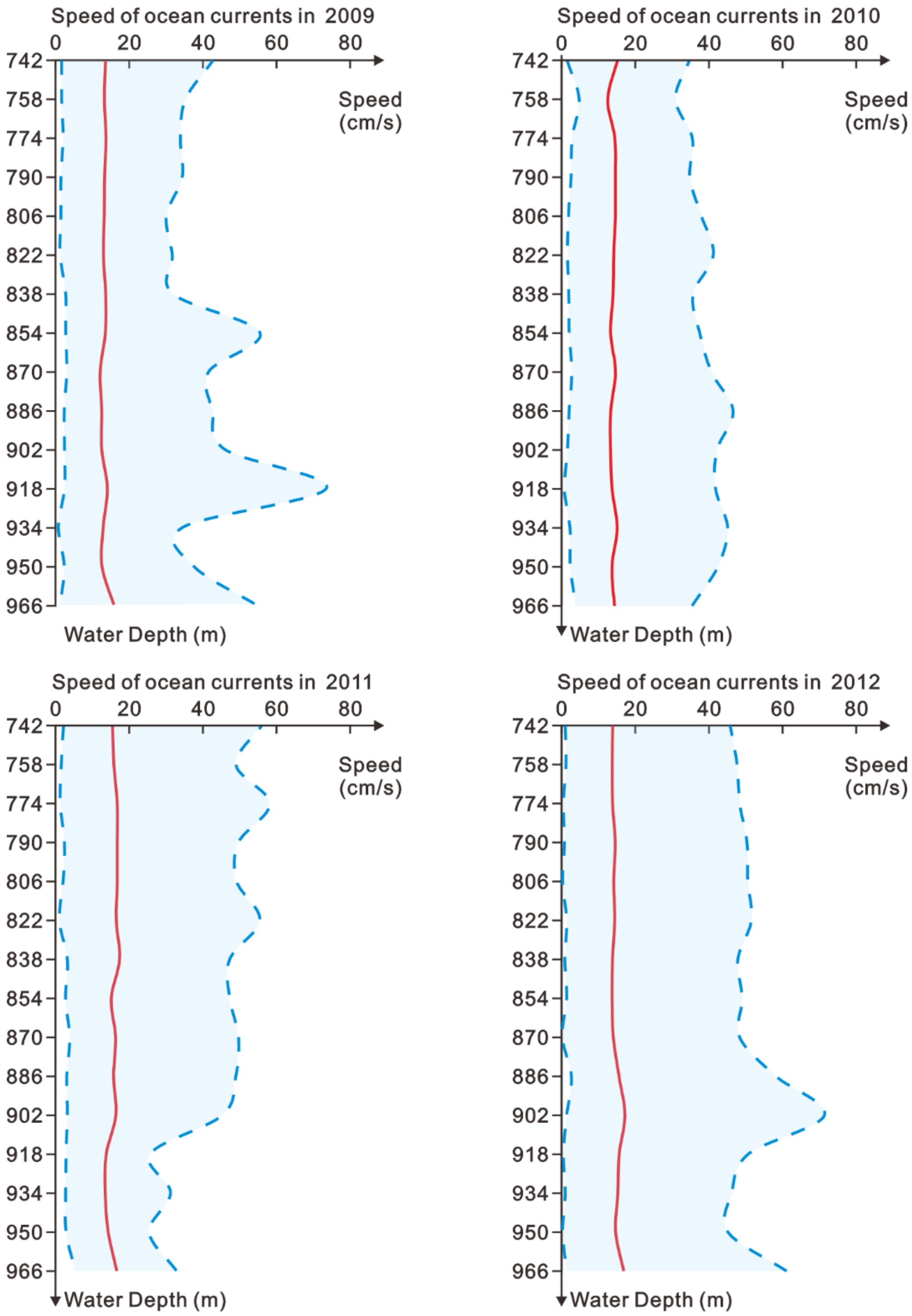

Figure S9. Profiles show the speed of ocean currents between the water depth of 742 and 966 m, acquired with a vessel-mounted ADCP Ocean Surveyor 38 kHz in the western South China Sea (2009 – 2012) obtained from Yang et al. (2019). The red lines indicate the average value of the in-situ measured current speed at different water depths, with the locations shown in Figure 1a. The blue dashed lines in the left and right reveal the minimum and maximum value of current speed at these locations, respectively. The speed profiles reveal a complex water circulation, with average speeds ranging between 10 to 20 cm/s and maximum speeds reaching 80 cm/s, at water depths typical of the study area.

Table S1. Detailed morphological information for the alongslope and across-slope channels imaged in Figure 2d.

Channel	**A-A’**	**B-B’**	**C-C’**	**D-D’**	**E-E’**	**F-F’**	**G-G’**
Classification	Along-slope channel	Along-slope channel	Along-slope channel	Across-slope channel	Across-slope channel	Along-slope channel	Across-slope channel
Maturity	Mature stage	Immature stage	Intermediate stage	Mature stage	Immature stage	Mature stage	Intermediate stage
Bankfull height (average)	73 m	80 m	94 m	240 m	92 m	171 m	129 m
Bankfull width (average)	1.7 km	1.2 km	1.3 km	2.6 km	1.1 km	2.6 km	1.9 km
Water depth (average)	950 m	917 m	980 m	798 m	770 m	745 m	802 m
Gradient of channel thalweg	0.51°	0.19°	0.40°	0.12°	0.85°	0.15°	0.17°
Roughness of thalweg (R_z*)	15 m	43 m	32 m	9 m	40 m	15 m	37 m

***Ps.** *the calculation of Roughness of thalweg (Rz) is based on the methodology of Sancaktar and Gomatam (2001):*

$$R_z = \frac{Z_1 + Z_2 + \cdots + Z_{n-1} + Z_n}{n}$$

References

Sancaktar, E., & R. Gomatam (2001), A study on the effects of surface roughness on the strength of single lap joints, *Journal of Adhesion Science and Technology*, **15**(1), 97-117. doi: 10.1163/156856101743346

Yang, Yuanzheng., Xu. C, Li. S, & He. Y (2019), Ship-mounted ADCP data for ocean currents in the South China Sea (2009–2012). doi: 10.11922/csdata.2019.0006.zh